Activity-dependent BDNF release and TRPC signaling is impaired in hippocampal neurons of *Mecp2* mutant mice

Wei Li[a], Gaston Calfa[a,1], Jennifer Larimore[b], and Lucas Pozzo-Miller[a,2]

[a]Department of Neurobiology, Civitan International Research Center, The University of Alabama at Birmingham, Birmingham, AL 35294; and [b]Biology Department and Neuroscience Program, Agnes Scott College, Decatur, GA 30030

Edited* by Mu-Ming Poo, University of California, Berkeley, CA, and approved September 4, 2012 (received for review March 28, 2012)

Dysfunction of the neurotrophin brain-derived neurotrophic factor (BDNF) is implicated in Rett syndrome (RTT), but the state of its releasable pool and downstream signaling in mice lacking methyl-CpG-binding protein-2 (*Mecp2*) is unknown. Here, we show that membrane currents and dendritic Ca^{2+} signals evoked by recombinant BDNF or an activator of diacylglycerol (DAG)-sensitive transient receptor potential canonical (TRPC) channels are impaired in CA3 pyramidal neurons of symptomatic *Mecp2* mutant mice. TRPC3 and TRPC6 mRNA and protein levels are lower in *Mecp2* mutant hippocampus, and chromatin immunoprecipitation (ChIP) identified *Trpc3* as a target of MeCP2 transcriptional regulation. BDNF mRNA and protein levels are also lower in *Mecp2* mutant hippocampus and dentate gyrus granule cells, which is reflected in impaired activity-dependent release of endogenous BDNF estimated from TRPC currents and dendritic Ca^{2+} signals in CA3 pyramidal neurons. These results identify the gene encoding TRPC3 channels as a MeCP2 target and suggest a potential therapeutic strategy to boost impaired BDNF signaling in RTT.

Rett syndrome (RTT) is caused by loss-of-function mutations in *MECP2*, encoding methyl-CpG-binding protein 2 (1), which regulates expression of multiple genes, including *Bdnf* (2), a modulator of activity-dependent development, function, and plasticity of CNS synapses (3). BDNF dysfunction likely accounts for sensory and motor abnormalities in RTT, including breathing irregularities (4). However, the underlying molecular mechanisms of BDNF dysfunction are unknown. Recombinant BDNF activates a slow nonselective cationic current (I_{BDNF}) in pontine neurons and hippocampal pyramidal neurons, which is mediated by TRPC3–containing channels downstream of tropomyosin-related kinase B (TrkB)/phospholipase C γ (PLCγ) activation (5, 6). In addition, theta-burst stimulation (TBS) of afferent fibers evokes TRPC-like currents in CA1 and CA3 pyramidal neurons that are sensitive to extracellular BDNF scavenging with TrkB-IgG- and shRNA-mediated TRPC3 knockdown (6, 7). Considering that TRPC3 and TRPC6 form heteromultimers (8) and are members of the PLCγ-coupled TRPC subfamily activated by DAG (9) and that both were identified in a comparative microarray study of *Mecp2* null and *MECP2*-overexpressing mouse hypothalami (2), we investigated BDNF signaling through TRPC3/6 channels in CA3 pyramidal neurons of male symptomatic *Mecp2* mutant mice ($Mecp2^{-/y}$; Jaenisch strain) (10).

Results and Discussion

Recombinant mature BDNF was pressure-applied from a glass pipette aimed to the apical dendrites of CA3 pyramidal neurons in the presence of TTX to evoke I_{BDNF} and associated dendritic Ca^{2+} signals, as observed in pontine and hippocampal pyramidal neurons (5, 6, 11). A single 30-s BDNF application evoked significantly smaller I_{BDNF} and dendritic Ca^{2+} signals in *Mecp2* mutant neurons from P40–60 male mice, which are in the symptomatic stage (wild type $n = 12$ cells/4 mice; $Mecp2^{-/y}$ $n = 8$ cells/4 mice; $P = 0.018$; Mann–Whitney test; Fig. 1 *A* and *B*; *SI Materials and Methods*). The relationship between I_{BDNF} and dendritic Ca^{2+} signals exhibits a significant linear relationship in neurons from both genotypes (wild type $n = 7$ cells/2 mice, $r = 0.617$, $P = 0.0362$; $Mecp2^{-/y}$ $n = 7$ cells/2 mice, $r = 0.648$, $P = 0.028$), whereas the correlation between groups was not statistically different ($P = 0.529$; analysis of covariance), suggesting that both features of BDNF-induced responses are equally affected by *Mecp2* deletion (Fig. 1 *C* and *D*). Consistent with the developmental nature of RTT, BDNF-induced currents and dendritic Ca^{2+} signals in *Mecp2* mutant neurons were not significantly affected in P16–17 mice (wild type n = 3 cells/1 mouse; $Mecp2^{-/y}$ n = 3 cells/1 mouse; I_{BDNF}, $P = 0.71$; fura-2 ratio, $P = 0.68$; Mann–Whitney test; Fig. S1*C*), a stage before the appearance of overt neurological symptoms.

Because the TRPC3-containing channels known to be necessary for the expression of I_{BDNF} (5–7) are activated by PLCγ-derived DAG (12), we next compared responses evoked by single 30-s applications of the DAG analog 1,2-Dioctanoyl-*sn*-glycerol (DOG) to apical dendrites of CA3 pyramidal neurons. As previously shown for another DAG analog (1-oleoyl-2-acetyl-*sn*-glycerol, OAG) in pontine and hippocampal CA1 pyramidal neurons (5, 6), DOG also evoked membrane currents (I_{DOG}) and dendritic Ca^{2+} signals in CA3 pyramidal neurons (Fig. 1*E*) with a time course similar to those evoked by recombinant BDNF (Fig. S1 *A* and *B*). Importantly, DOG-evoked currents and dendritic Ca^{2+} signals were significantly smaller in $Mecp2^{-/y}$ neurons (wild type $n = 15$ cells/8 mice; $Mecp2^{-/y}$ $n = 15$ cells/7 mice; $P = 0.0008$ both I_{BDNF} and fura-2 ratio; Mann–Whitney test; Fig. 1*E*). DOG-evoked currents and dendritic Ca^{2+} signals showed a significant linear relationship in both genotypes (wild type $r = 0.64$, $P = 0.0003$; $Mecp2^{-/y}$ $r = 0.28$, $P = 0.038$), but their correlation was not statistically different between genotypes ($P = 0.079$; analysis of covariance), suggesting that both features of DOG-induced responses are equally affected by *Mecp2* deletion (Fig. 1*F*), as is the case for BDNF-mediated signals (Fig. 1*D*).

Consistent with the above physiological observations, using well-characterized antibodies for Western immunoblots, we found that BDNF, TRPC3, and TRPC6 protein levels were significantly lower in the hippocampus (Fig. 2 *A–C*), as well as several other brain regions of $Mecp2^{-/y}$ mice (Fig. S2 *A* and *B*). Western blots for BDNF show different bands, which represent

Author contributions: W.L., G.C., and L.P.-M. designed research; W.L., G.C., and J.L. performed research; W.L., J.L., and L.P.-M. analyzed data; and W.L., G.C., J.L., and L.P.-M. wrote the paper.

The authors declare no conflict of interest.

*This Direct Submission article had a prearranged editor.

[1]Present address: Instituto de Farmacología Experimental de Córdoba (IFEC), Consejo Nacional de Investigaciones Científicas y Técnicas (CONICET), Departamento de Farmacología, Facultad de Ciencias Químicas, Universidad Nacional de Córdoba, Córdoba (5000) Argentina.

[2]To whom correspondence should be addressed. E-mail: lucaspm@uab.edu

This article contains supporting information online at www.pnas.org/lookup/suppl/doi:10.1073/pnas.1205271109/-/DCSupplemental.

NEUROSCIENCE

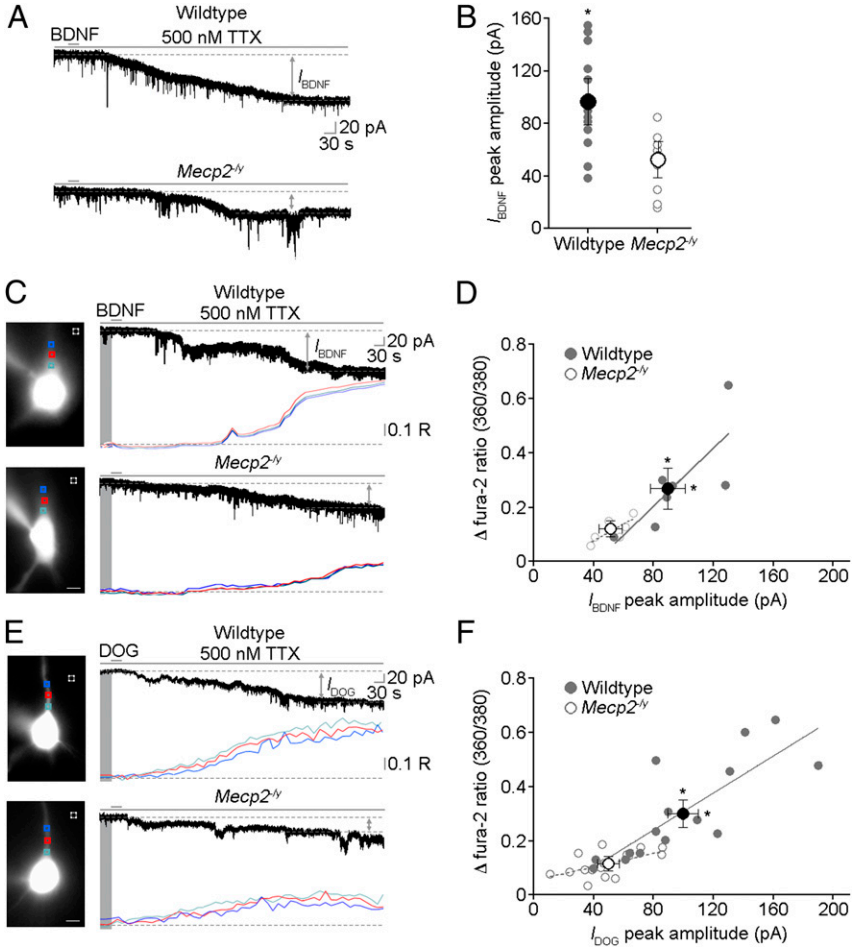

Fig. 1. Membrane currents and Ca^{2+} signals evoked by recombinant BDNF and a TRPC3/6 channel activator are impaired in symptomatic male *Mecp2* mutant mice. (*A*) Representative examples of I_{BDNF} evoked by single 30-s applications of recombinant BDNF to apical dendrites of CA3 pyramidal neurons in the presence of 500 nM TTX (*SI Materials and Methods*). (*B*) Peak I_{BDNF} amplitude is smaller in *Mecp2*$^{-/y}$ neurons. (*C*) Representative examples of I_{BDNF} and simultaneous dendritic Ca^{2+} signals evoked in CA3 pyramidal neurons in the presence of 500 nM TTX (images are neurons loaded with fura-2 and excited at 380 nm; scale bar: 10 μm; R is the 360/380-nm ratio of fura-2 emission). (*D*) Correlation between changes (δ) in fura-2 360/380 ratios and peak I_{BDNF} amplitudes in wild type (gray filled circles) and *Mecp2*$^{-/y}$ neurons (gray open circles). Average changes of fura-2 360/380 ratios and peak I_{BDNF} amplitudes are smaller in *Mecp2*$^{-/y}$ neurons (dark open circle) than in wild-type neurons (dark filled circle). (*E*) Representative examples of currents (I_{DOG}) and Ca^{2+} signals evoked by single 30-s applications of DOG to apical dendrites of CA3 pyramidal neurons in the presence of 500 nM TTX (images are neurons loaded with fura-2 and excited at 380 nm; scale bar: 10 μm). (*F*) Correlation between changes of fura-2 360/380 ratios and peak I_{DOG} amplitudes in wild-type (gray filled circles) and *Mecp2*$^{-/y}$ neurons (gray open circles). Average changes of fura-2 360/380 ratios and peak I_{DOG} amplitudes are smaller in *Mecp2*$^{-/y}$ neurons (dark open circle) than in wild-type neurons (dark filled circle). All data in this and next figures are mean ± SEM; **P* < 0.05 wild type vs. *Mecp2*$^{-/y}$.

monomeric mature BDNF (~14 kDa) and various precursor forms of BDNF, as previously described (13). Mature BDNF bands are the only ones that appear when we performed Western blots with this anti-BDNF antibody on samples of human recombinant mature BDNF at different concentrations, and are completely absent when the anti-BDNF antibody is preabsorbed with recombinant BDNF (Fig. 2*A*). In addition, hippocampal samples from *Mecp2*$^{-/y}$ mice expressed lower levels of *Bdnf* (n = 8, P = 0.045; two-tailed unpaired t test), *Trpc3* (n = 8, P = 0.0074), and *Trpc6* (n = 8, P = 0.0025) mRNAs (Fig. 2 *D*–*F*). These lower *Bdnf*, *Trpc3*, and *Trpc6* expression levels are consistent with a comparative microarray study of hypothalamic samples from *Mecp2* null and *MECP2*-overexpressing mice (2). Furthermore, the levels of BDNF immunoreactivity in the mossy fiber (MF) tract along CA3 *stratum lucidum*—the region of highest BDNF expression in the brain (14, 15)—were significantly lower in *Mecp2* mutant mice (wild type n = 9 mice; *Mecp2*$^{-/y}$ n = 8 mice; P = 0.0002, Mann–Whitney test; Fig. 2*G*).

In agreement with previous reports (16, 17), our chromatin immunoprecipitation (ChIP) assays showed that MeCP2 binds to *Bdnf* at ~0–300 Kb upstream of the transcription start site in hippocampal samples from wild-type mice, whereas the interaction is minimal in *Mecp2* mutant samples (Fig. S2*D*). Next, chromatin fragments immunoprecipitated by MeCP2 antibodies from cerebral cortical and hippocampal samples were amplified by PCR using specific primer pairs spanning ~4.2 kb of the *Trpc3* gene regulatory region (Fig. 2*H*). We found enriched MeCP2 occupancy at 2.4–3.2 kb upstream of the *Trpc3* transcription start site in wild-type samples but no appreciable binding in samples from *Mecp2* mutant mice. On the other hand, a similar ChIP assay using specific primers pairs spanning ~4.0 kb of the *Trpc6* gene regulatory region failed to detect significant MeCP2 occupancy in wild-type or *Mecp2* mutant samples (Fig. S2*E*), suggesting that the reduced levels of TRPC6 mRNA and protein are due to indirect consequences of *Mecp2* deletion. These results strongly suggest that the lower levels of *Trpc3* mRNA in *Mecp2*

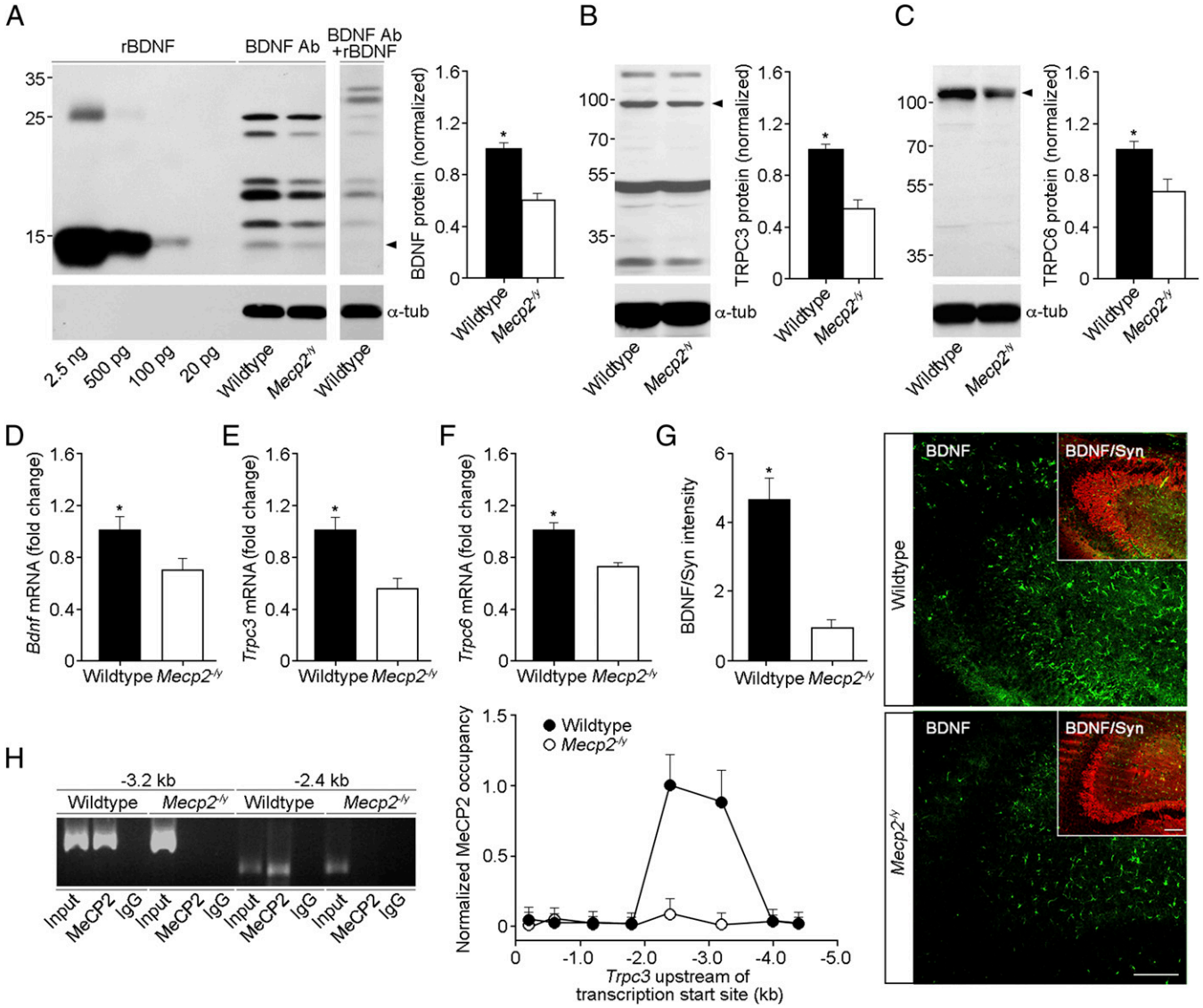

Fig. 2. Expression of BDNF, TRPC3, and TRPC6 is impaired in several brain regions of symptomatic male *Mecp2* mutant mice. (*A–C*) Representative examples of Western immunoblots in hippocampal samples from wild type and *Mecp2*$^{-/y}$ assessed for BDNF (*A*), TRPC3 (*B*), and TRPC6 (*C*) protein levels. (*A*) Western immunoblots were performed in samples of recombinant mature met-BDNF at different concentrations (*Left*), in hippocampal lysates from wild-type and *Mecp2*$^{-/y}$ mice (*Center*), and in hippocampal lysates using primary antibodies preabsorbed with recombinant BDNF (*Right*). Results from quantitative analyses (using α-tubulin as loading control) and shown to the right of the blots demonstrate lower BDNF (*A*), TRPC3 (*B*), and TRPC6 (*C*) levels in the hippocampus of *Mecp2*$^{-/y}$ mice (BDNF, $n = 10$ mice, $P < 0.0001$; TRPC3, $n = 8$ mice, $P < 0.0001$; TRPC6, $n = 7$ mice, $P = 0.018$; two-tailed unpaired *t* test). (*D–F*) Real-time RT-PCR analyses demonstrate lower *Bdnf*, *Trpc3*, and *Trpc6* mRNA levels in the hippocampus of *Mecp2*$^{-/y}$ mice (*Bdnf*, $n = 8$ mice, $P = 0.045$; *Trpc3*, $n = 8$ mice, $P = 0.0074$; *Trpc6*, $n = 8$ mice, $P = 0.0025$; two-tailed unpaired *t* test). (*G*, *Left*) Semiquantitative analysis of BDNF immunoreactivity in the MF tract in CA3 *stratum lucidum*. (*Right*) Representative examples of BDNF and synaptophysin (*Inset*) IHC in area CA3 of hippocampal sections from wild-type (*Upper*) and *Mecp2* mutant (*Lower*) mice. It should be noted that the intensity of synaptophysin immunoreactivity is comparable between genotypes (Scale bar: 10 μm). (*H*, *Left*) Representative examples of agarose gel electrophoresis following ChIP show strong association between MeCP2 and *Trpc3* gene in samples from wild-type mice, which is absent in control IgG and *Mecp2* mutants. (*Right*) Mapping of MeCP2 occupancy at 0.2–4.4 kb upstream of the transcription start site of the *Trpc3* gene. *$P < 0.05$, wild type vs. *Mecp2*$^{-/y}$.

mutant brains are due to direct MeCP2 transcriptional control, identifying *Trpc3* as a gene target of MeCP2 regulation.

What is the physiological consequence of such reduced BDNF, TRPC3, and TRPC6 protein levels in *Mecp2*$^{-/y}$ mice? To address this question, we used membrane currents and dendritic Ca^{2+} signals mediated by TRPC channels as indirect readouts of activity-dependent release of endogenous BDNF (6, 7). A single TBS train to afferent MFs in the presence of a mixture of ionotropic and metabotropic glutamate and GABA receptor antagonists evoked an inward current (MF-I_{BDNF}) in CA3 pyramidal neurons, which outlasted the afferent TBS (Fig. 3*A*; *SI Materials and Methods*), as seen in rat hippocampal slices (7). These TBS-evoked currents have different delay and onset kinetics than the ones evoked by pressure application of recombinant BDNF from a glass pipette onto large areas of the dendritic tree of CA3 pyramidal neurons in slices (Fig. 1 *A* and *B*). The parsimonious explanation for these kinetic differences is that the diffusion of recombinant BDNF from a puffer pipette is very different from the diffusion from BDNF-containing dense-core vesicles within MF terminals. The puffer pipette was positioned several tens of microns above the slice surface to avoid pressure-related mechanical artifacts, and the MF terminals are right across the

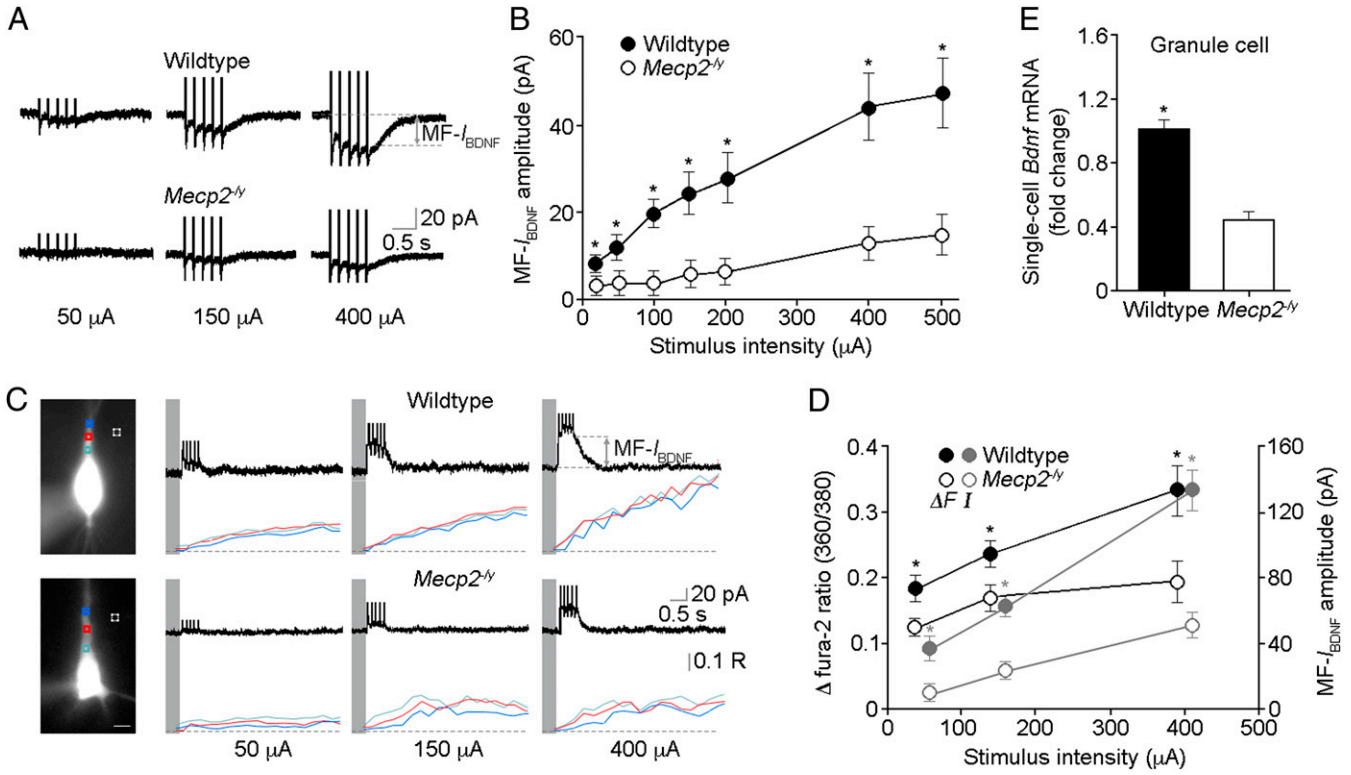

Fig. 3. Membrane currents and Ca^{2+} signals evoked by stimulation of presynaptic MFs are impaired in symptomatic male *Mecp2* mutant mice. (*A*) Representative MF-I_{BDNF} in CA3 pyramidal neurons of wild-type and *Mecp2*$^{-/y}$ mice evoked by TBS of afferent MFs in the presence of a mixture of glutamatergic and GABAergic receptor antagonists (*SI Materials and Methods*). (*B*) Input-output curves of MF-I_{BDNF}. (*C*) Representative images of fura-2-loaded neurons during simultaneous whole-cell recording and Ca^{2+} imaging (380 nm excitation; scale bar: 10 μm; R is the 360/380-nm fura-2 ratio). Fura-2 360/380 ratios were measured from regions of interest (ROIs) over primary dendrites (color-coded in the traces at right); dashed squares are ROIs of background measurements. (*D*) Peak MF-I_{BDNF} amplitude and changes in fura-2 360/380 ratio plotted vs. afferent stimulus intensity. (*E*) Lower levels of *Bdnf* mRNA in individual *Mecp2*$^{-/y}$ granule cells of the dentate gyrus (single-cell real-time RT-PCR), which are presynaptic to CA3 pyramidal neurons in recordings of MF-induced I_{BDNF} (MF-I_{BDNF}). *$P < 0.05$, wild type vs. *Mecp2*$^{-/y}$.

postsynaptic CA3 neurons under recording. This puffer pipette arrangement introduces a delay and slows down the onset of the BDNF responses. It should be noted that membrane currents evoked in CA1 and CA3 pyramidal neurons by pressure application of recombinant BDNF have the same pharmacological profile as those evoked by afferent stimulation in the presence of the glutamatergic and GABAergic receptor antagonist mixture (6, 7).

Increasing stimulus intensities evoked MF-I_{BDNF} responses of progressively larger amplitude in both genotypes, but they were significantly smaller and with a faster decay time in *Mecp2* mutant neurons at all stimulus intensities (wild type $n = 25$ cells/8 mice; *Mecp2*$^{-/y}$ $n = 14$ cells/4 mice; $P < 0.05$ for all groups; Mann–Whitney test; Fig. 3*B*; Fig. S3 *B* and *C*). As with recombinant BDNF-induced I_{BDNF} in presymptomatic mice, there were no significant differences in MF-I_{BDNF} and dendritic Ca^{2+} signals in neurons from P16–17 mice (wild type n = 5 cells/2 mice; *Mecp2*$^{-/y}$ n = 5 cells/2 mice; $P = 0.42$ at 50 μA, $P = 0.31$ at 150 μA, $P = 0.22$ at 400 μA for MF-I_{BDNF}; $P = 0.31$ at 50 μA, $P = 0.15$ at 150 μA, $P = 0.54$ at 400 μA for fura-2 360/380-nm ratios; Mann–Whitney test; Fig. S3*D*). As we showed before in CA1 and CA3 pyramidal neurons of rat hippocampal slices (6, 7), sensitivity to the extracellular BDNF scavenger TrkB-IgG (1 μg/mL) confirmed that MF-I_{BDNF} requires activity-dependent BDNF release ($n = 7$ cells/4 mice, $P < 0.05$ for all groups; two-tailed Wilcoxon matched pairs test; Fig. S4*A*); as a control, a nonspecific human control IgG had no effect on MF-I_{BDNF} (Fig. S4*B*).

To reduce the contribution of voltage-gated Ca^{2+} channels during TBS of afferent MFs, we performed the next series of simultaneous whole-cell recordings and Ca^{2+} imaging at depolarized potentials (+40 mV) with the addition of the L-type Ca^{2+} channel blocker nimodipine in the antagonists mixture (18). Consistently, TBS of MFs evoked outward MF-I_{BDNF} responses (see I-V relationship in ref. 6) and accompanying dendritic Ca^{2+} signals, both of which were significantly smaller in *Mecp2* mutant neurons at all stimulus intensities (wild type $n = 17$ cells/8 mice; *Mecp2*$^{-/y}$ $n = 10$ cells/5 mice; $P < 0.0001$ at 50 μA, $P = 0.0002$ at 150 μA, $P < 0.0001$ at 400 μA for MF-I_{BDNF}; $P = 0.029$ at 50 μA, $P = 0.032$ at 150 μA, $P = 0.019$ at 400 μA for fura-2 360/380nm ratios; Mann–Whitney test; Fig. 3 *C* and *D*). Together, these results demonstrate that MF-I_{BDNF} and associated dendritic Ca^{2+} signals that are sensitive to extracellular BDNF quenching are impaired in *Mecp2* mutant neurons.

Smaller MF-I_{BDNF} could be due to reduced presynaptic BDNF release, impaired postsynaptic TrkB-TRPC signaling, or a combination of both. Compared with the threefold decrease in membrane currents evoked by stimulation of afferent MFs (Fig. 3*B*), I_{BDNF} evoked by recombinant BDNF is only ~twofold smaller in *Mecp2* mutant neurons (Fig. 1*B*), which strongly suggests that activity-dependent release of endogenous BDNF from presynaptic MFs is affected in *Mecp2*$^{-/y}$ mice. Indeed, single-cell real-time RT-PCR demonstrated that *Mecp2* mutant granule cells of the dentate gyrus (which give rise to MFs) expressed lower levels of *Bdnf* mRNA ($n = 12$, $P < 0.0001$; two-tailed unpaired *t* test; Fig. 3*E*; Fig. S2*F*). Consistent with lower levels of BDNF in the extracellular space following TBS of MFs in *Mecp2* mutant slices, a subeffective concentration of the BDNF scavenger TrkB-IgG (0.25 μg/mL) completely blocked MF-I_{BDNF} in *Mecp2* mutant neurons, whereas MF-I_{BDNF} was still detected—albeit reduced—in wild-type neurons (Fig. S5*A*). As a complementary assay for activity-dependent BDNF release, Western blots for phosphorylated

TrkB, PLCγ1, Erk, and Akt in slices that received three TBS trains to MFs in CA3 *stratum lucidum* (30 s intervals) showed no significant increases in either wild-type or *Mecp2*$^{-/y}$ mice (Fig. S5 *B–E*). To avoid the inevitable dilution factor in homogenized hippocampal slices prepared for Western blots, we then performed semiquantitative immunohistochemistry (IHC) with antibodies against phospho-TrkB receptors in slices stimulated as above right before fixation (or were fixed without stimulation, as naïve controls). The intensity of phospho-TrkB staining throughout the MF tract in CA3 *stratum lucidum* was significantly higher in stimulated slices than in naïve control slices (wild-type control $n = 11$ sections/5 mice; wild-type TBS $n = 8$ sections/5 mice; $P = 0.005$, Mann–Whitney test; Fig. 4). Consistently, the intensity of phospho-TrkB IHC after stimulation was significantly lower in *Mecp2* mutant slices than in wild-type slices (*Mecp2*$^{-/y}$ TBS $n = 7$ sections/5 mice; $P = 0.037$; Fig. 4). Furthermore, preincubation with TrkB-IgG (1 μg/mL) prevented the TBS-evoked increase in phospho-TrkB staining (Fig. 4), strongly suggesting that it reflects activity-dependent BDNF release. These observations support the view that activity-dependent BDNF release is impaired in hippocampal slices from *Mecp2* mutant mice.

Altogether, our findings demonstrate impaired BDNF release from presynaptic MFs and postsynaptic TRPC3/6 signaling in *Mecp2* mutant mice, revealing a cellular phenotype that certainly contributes to hippocampal dysfunction in *Mecp2* mutant mice as well as to RTT etiology. BDNF-evoked TRPC3 activation and the resultant Ca^{2+} entry are critical for growth-cone guidance and neuronal survival (19, 20). Dysfunction of this signaling pathway could alter neuronal structure and function and affect the excitation-inhibition balance of neuronal networks as observed in *Mecp2* mutant mice (21) and RTT individuals (22). Lastly, BNDF-induced currents and Ca^{2+} signals are potentially useful as physiological bioassays for the screening and evaluation of therapeutic compounds that enhance BDNF release or boost TRPC3/6 channel function in *Mecp2* mutant mice.

Materials and Methods

Animals. Experimental subjects were hemizygous *Mecp2*$^{tm1.1Jae}$ mutant males of the Jaenisch strain (termed *Mecp2*$^{-/y}$) aged between postnatal days 16 and 17 for the presymptomatic stage and 40 and 60 for the symptomatic stage, when they exhibited RTT-like motor symptoms such as hypoactivity, hind-limb clasping, and reflex impairments (10); age-matched wild-type male littermates were used as the controls. Animals were handled and housed according to the Committee on Laboratory Animal Resources of the National Institutes of Health. All experimental protocols were annually reviewed and approved by the Institutional Animals Care and Use Committee of the University of Alabama at Birmingham.

Acute Hippocampal Slices. Mice were anesthetized with an intraperitoneal (i.p.) injection of a solution of ketamine at 100 mg/mL (wt/vol) per kg of body weight and transcardially perfused with ice-cold "cutting" artificial cerebrospinal

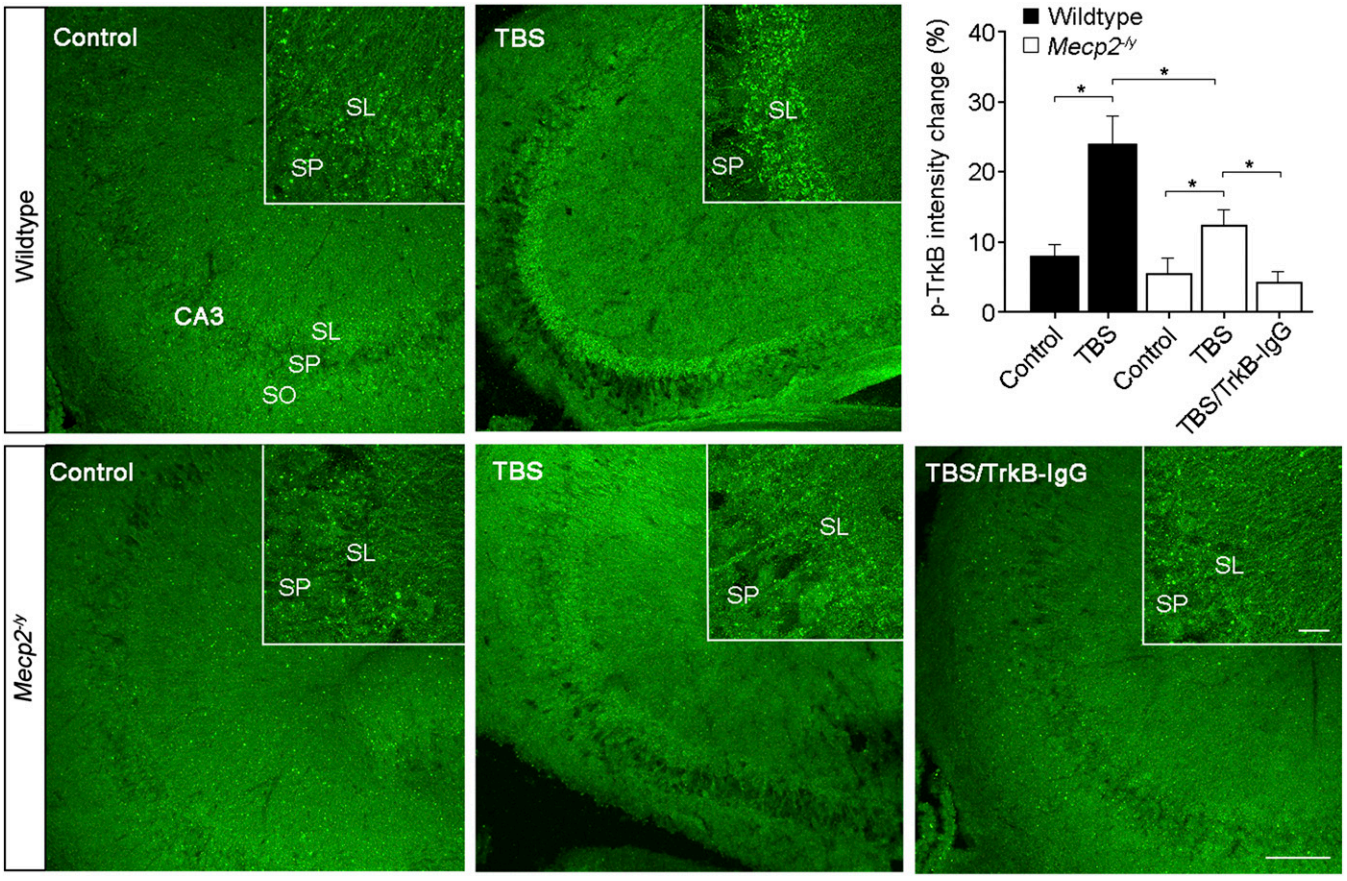

Fig. 4. Activation of TrkB receptors in CA3 *stratum lucidum* following stimulation of MF is impaired in symptomatic male *Mecp2* mutant mice. (*Left*) Representative examples of immunohistochemical labeling with antibodies against phospho-TrkB receptors in acute slices before (control) and after three sets of TBS to the MF tract in CA3 *stratum lucidum* in wild-type (*Upper*) and *Mecp2* mutant mice (*Lower*). (*Right*) Semiquantitative analysis of phospho-TrkB immunoreactivity. The intensity of phospho-TrkB IHC staining after stimulation was significantly lower in *Mecp2* mutant slices than in wild-type slices, although both were increased compared with the naïve controls of the corresponding genotype. Preincubation with the BDNF scavenger TrkB-IgG (1 μg/mL) completely abolished the increase in phospho-TrkB immunoreactivity after TBS in *Mecp2*$^{-/y}$ slices (*Lower Right*). Inset shows higher magnification images from the corresponding sections. SP, *stratum pyramidale*; SL, *stratum lucidum*; SO, *stratum oriens*. (Scale bar: 10μm). *$P < 0.05$.

fluid (aCSF) containing (mM): 87 NaCl, 2.5 KCl, 0.5 $CaCl_2$, 7 $MgCl_2$, 1.25 NaH_2PO_4, 25 $NaHCO_3$, 25 glucose, and 75 sucrose, which was bubbled with 95% O_2/5% CO_2. Hippocampal slices were obtained following standard procedures, as described (21) (*SI Materials and Methods*).

Simultaneous Electrophysiology and Ca^{2+} Imaging. Whole-cell recordings and Ca^{2+} imaging were obtained from visualized CA3 pyramidal neurons after dialysis with intracellular solution containing fura-2, following standard procedures, as described (18) (*SI Materials and Methods*). Recombinant mature BDNF and DOG were pressure-applied from glass pipettes, whereas afferent MFs were stimulated with theta glass pipettes filled with aCSF, as described (6, 7, 11).

Real-Time Reverse Transcription-PCR, Western Immunoblots, Immunohistochemistry, and Confocal Microscopy. Total RNA was extracted from whole hippocampi or from single cells after whole-cell recording, and Reverse Transcription (RT)-PCR was performed following standard procedures. Western immunoblots were also performed following standard procedures. IHC on hippocampal sections from perfused-fixed brains were prepared with a vibrating microtome, acute slices were fixed after afferent stimulation, and semiquantitative confocal microscopy was performed following standard procedures. For details, see *SI Materials and Methods*.

ChIP. ChIP was performed on cerebral cortical and hippocampal samples as described previously with some modifications (*SI Materials and Methods*) (23). PCR was used to amplify different *Bdnf*, *Trpc3*, and *Trpc6* gene regulatory regions, and maximal MeCP2 occupancy was calculated from threshold cycle (Ct) for both wild-type and *Mecp2* mutant mice.

Statistical Analyses. Data for input-output curves of MF-I_{BDNF} and fura-2 ratios and for amplitudes and time courses of membrane currents and fura-2 ratios evoked by recombinant BDNF and DOG were analyzed with one-way repeated measurements ANOVA using Prism software package (GraphPad Software). Specific comparisons between wild-type and *Mecp2*$^{-/y}$ mice were made using Mann–Whitney test. Data for TrkB-IgG and IgG treatments were analyzed with two-tailed Wilcoxon matched pairs test. Data for Western blots, real-time RT-PCR, and IHC were analyzed with two-tailed unpaired *t* test, except otherwise indicated. Linear regressions were made for correlation between fura-2 ratios and peak amplitudes of BDNF- and DOG-evoked currents, and analysis of covariance was used for comparisons between regression lines. Data are shown as the mean ± SEM. Statistical differences were considered significant at $P < 0.05$.

ACKNOWLEDGMENTS. We thank Takafumi Inoue (Waseda University, Tokyo, Japan) for data acquisition and analysis software and Farah Lubin (University of Alabama at Birmingham) for advice and technical assistance with RT-PCR. This work was supported by National Institutes of Health Grants NS-065027 and NS-40593 (to L.P.-M.) and by Postdoctoral Fellowships IRSF-2824 (to W.L.) and IRSF-0804 (to G.C.) from the International Rett Syndrome Foundation. The Alabama Neuroscience Blueprint Core Center (P30-NS57098), the UAB Intellectual and Developmental Disabilities Research Center (P30-HD38985), and the UAB Neuroscience Core (P30-NS47466) provided instrumentation.

1. Amir RE, et al. (1999) Rett syndrome is caused by mutations in X-linked MECP2, encoding methyl-CpG-binding protein 2. *Nat Genet* 23:185–188.
2. Chahrour M, et al. (2008) MeCP2, a key contributor to neurological disease, activates and represses transcription. *Science* 320:1224–1229.
3. Poo MM (2001) Neurotrophins as synaptic modulators. *Nat Rev Neurosci* 2:24–32.
4. Kline DD, Ogier M, Kunze DL, Katz DM (2010) Exogenous brain-derived neurotrophic factor rescues synaptic dysfunction in Mecp2-null mice. *J Neurosci* 30:5303–5310.
5. Li HS, Xu XZ, Montell C (1999) Activation of a TRPC3-dependent cation current through the neurotrophin BDNF. *Neuron* 24:261–273.
6. Amaral MD, Pozzo-Miller L (2007) TRPC3 channels are necessary for brain-derived neurotrophic factor to activate a nonselective cationic current and to induce dendritic spine formation. *J Neurosci* 27:5179–5189.
7. Li Y, Calfa G, Inoue T, Amaral MD, Pozzo-Miller L (2010) Activity-dependent release of endogenous BDNF from mossy fibers evokes a TRPC3 current and Ca2+ elevations in CA3 pyramidal neurons. *J Neurophysiol* 103:2846–2856.
8. Ramsey IS, Delling M, Clapham DE (2006) An introduction to TRP channels. *Annu Rev Physiol* 68:619–647.
9. Hofmann T, et al. (1999) Direct activation of human TRPC6 and TRPC3 channels by diacylglycerol. *Nature* 397:259–263.
10. Chen RZ, Akbarian S, Tudor M, Jaenisch R (2001) Deficiency of methyl-CpG binding protein-2 in CNS neurons results in a Rett-like phenotype in mice. *Nat Genet* 27:327–331.
11. Amaral MD, Pozzo-Miller L (2007) BDNF induces calcium elevations associated with I_{BDNF}, a nonselective cationic current mediated by TRPC channels. *J Neurophysiol* 98: 2476–2482.
12. Putney JW (2005) Physiological mechanisms of TRPC activation. *Pflugers Arch* 451: 29–34.
13. Mowla SJ, et al. (2001) Biosynthesis and post-translational processing of the precursor to brain-derived neurotrophic factor. *J Biol Chem* 276:12660–12666.
14. Danzer SC, McNamara JO (2004) Localization of brain-derived neurotrophic factor to distinct terminals of mossy fiber axons implies regulation of both excitation and feedforward inhibition of CA3 pyramidal cells. *J Neurosci* 24:11346–11355.
15. Dieni S, et al. (2012) BDNF and its pro-peptide are stored in presynaptic dense core vesicles in brain neurons. *J Cell Biol* 196:775–788.
16. Chen WG, et al. (2003) Derepression of BDNF transcription involves calcium-dependent phosphorylation of MeCP2. *Science* 302:885–889.
17. Martinowich K, et al. (2003) DNA methylation-related chromatin remodeling in activity-dependent BDNF gene regulation. *Science* 302:890–893.
18. Pozzo Miller LD, Petrozzino JJ, Golarai G, Connor JA (1996) Ca2+ release from intracellular stores induced by afferent stimulation of CA3 pyramidal neurons in hippocampal slices. *J Neurophysiol* 76(1):554–562.
19. Li Y, et al. (2005) Essential role of TRPC channels in the guidance of nerve growth cones by brain-derived neurotrophic factor. *Nature* 434:894–898.
20. Jia Y, Zhou J, Tai Y, Wang Y (2007) TRPC channels promote cerebellar granule neuron survival. *Nat Neurosci* 10:559–567.
21. Calfa G, Hablitz JJ, Pozzo-Miller L (2011) Network hyperexcitability in hippocampal slices from Mecp2 mutant mice revealed by voltage-sensitive dye imaging. *J Neurophysiol* 105:1768–1784.
22. Glaze DG, et al. (2010) Epilepsy and the natural history of Rett syndrome. *Neurology* 74:909–912.
23. Chao HT, et al. (2010) Dysfunction in GABA signalling mediates autism-like stereotypies and Rett syndrome phenotypes. *Nature* 468:263–269.